J Comput Neurosci
DOI 10.1007/s10827-014-0535-3

Encoding whisker deflection velocity within the rodent barrel cortex using phase-delayed inhibition

Runjing Liu · Mainak Patel · Badal Joshi

Received: 24 August 2014 / Revised: 23 September 2014 / Accepted: 26 September 2014

Abstract The primary sensory feature represented within the rodent barrel cortex is the velocity with which a whisker has been deflected. Whisker deflection velocity is encoded within the thalamus via population synchrony (higher deflection velocities entail greater synchrony among the corresponding thalamic population). Thalamic (TC) cells project to regular spiking (RS) cells within the barrel cortex, as well as to inhibitory cortical fast-spiking (FS) neurons, which in turn project to RS cells. Thus, TC spikes result in EPSPs followed, with a small time lag, by IPSPs within an RS cell, and hence the RS cell decodes TC population synchrony by employing a phase-delayed inhibition synchrony detection scheme. As whisker deflection velocity is increased, the probability that an RS cell spikes rises, while jitter in the timing of RS cell spikes remains constant. Furthermore, repeated whisker deflections with fixed velocity lead to system adaptation – TC→RS, TC→FS, and FS→RS synapses all weaken substantially, leading to a smaller probability of spiking of the RS cell and increased jitter in the timing of RS cell spikes. Interestingly, RS cell activity is better able to distinguish among different whisker deflection velocities after adaptation. In this work, we construct a biophysical model of a basic 'building block' of barrel cortex – the feedforward circuit consisting of TC cells, FS cells, and a single RS cell – and we examine the ability of the purely feedforward circuit to explain the experimental data on RS cell spiking probability, jitter, adaptation, and deflection velocity discrimination. Moreover, we study the contribution of the phase-delayed inhibition network structure to the ability of an RS cell to decode whisker deflection velocity encoded via TC population synchrony.

Keywords Phase-delayed inhibition · Feedforward inhibition · Barrel cortex · Neuronal networks · Synchrony detection · Computational neuroscience · Network structure and function · Adaptation · Whisker deflection velocity

1 Introduction

Synchrony is a pervasive feature of neural systems, implying that synchrony may be a strategy commonly employed by neuronal networks to encode and relay information (Eckhorn 1994; Friedrich et al. 2004; Gray 1994; Laurent and Davidowitz 1994; Patel et al. 2009, 2013; Marthy and Fetz 1992). However, in order for the brain to use synchrony as a coding tool, a neural mechanism must exist that is capable of decoding the activity of a population of cells representing information by firing synchronously. There are two simple, biologically plausible mechanisms for creating such a decoder: 1) a decoder neuron with a high spike threshold (relative to the strength of individual inputs), and 2) a decoder neuron that receives phase-delayed inhibition. A decoder with a high threshold (Fig. 1A) detects synchrony by virtue of the fact that a large proportion of its inputs (the encoders) must fire in unison in order for the decoder to

Action Editor: David Golomb

R. Liu
Duke University, Durham, NC USA

M. Patel (✉)
Department of Mathematics, College of William and Mary, Williamsburg, VA USA
e-mail: mjpatel@wm.edu

B. Joshi
Department of Mathematics, California State University, San Marcos, CA USA

Published online: 05 October 2014

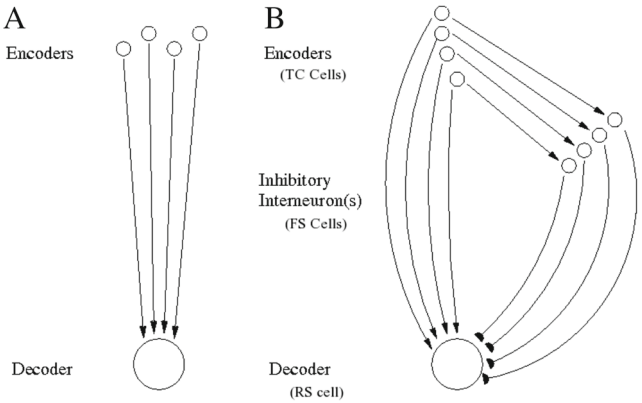

Fig. 1 Schematic of network architecture needed to implement synchrony decoding with a high spike threshold versus phase-delayed inhibition. **A** High spike threshold decoder. A set of excitatory encoder neurons innervate a decoder neuron with a high spiking threshold relative to the strength of encoder inputs. **B** Phase-delayed inhibition decoder. A set of excitatory encoder neurons innervate a set of inhibitory interneurons as well as sending convergent input to a decoder neuron. The decoder neuron also receives input from the inhibitory interneurons. Each excitatory encoder spike is followed, with a slight delay, by an inhibitory interneuron spike

cross spike threshold, and hence this decoder will be active only if this condition is satisfied.

The neural architecture underlying phase-delayed inhibition consists of a group of neurons (the encoders) that provide excitation to a decoder neuron, but en-route to the decoder the axons of the encoders send collaterals to a group of inhibitory interneurons, which in turn provide potent inhibitory input to the decoder (Fig. 1B). Thus, each excitatory input to the decoder is followed, with a temporal lag, by an inhibitory input. The intuition behind phase-delayed inhibition is clear; if the encoders spike haphazardly, then so do the inhibitory interneurons, and the read-out neuron remains covered in a blanket of unrelenting inhibition, unable to respond to the encoders. If, on the other hand, the encoders fire synchronously, then the decoder will receive aggregate excitation followed by pooled inhibition, allowing the decoder to respond to the encoders within the window of excitation.

Despite requiring a more complex architecture than a high spike threshold decoder, the phase-delayed inhibition motif exists as a means to detect synchrony in a myriad of neural systems, including the tectofugal pathway of the barn owl (Benowitz and Karten 2004; Deng and Rogers 1998; Sridharan et al. 2011; Patel and Reed 2013) and the parallel fiber-molecular layer-Purkinje cell circuit of the cerebellum (Mittmann et al. 2005), as well as in the hippocampus (Fricker and Miles 2000; Pouille and Scanziani 2001), auditory cortex (Wehr and Zador 2003), lateral geniculate nucleus of the thalamus (Blitz and Regehr 2005), and locust olfactory system (Jortner et al. 2007; Leitch et al. 1996; Perez-Orive et al. 2002), among others. In prior work (Patel and Joshi 2013; Joshi and Patel 2013), we study the difference between a synchrony decoder that uses phase-delayed inhibition versus one that employs a high spike threshold. We find that if the variable used to encode stimuli is synchrony, then, in a system of noisy encoders, phase-delayed inhibition allows for the construction of a more reliable and specific decoder than a high spike threshold scheme. In this study, we examine synchrony decoding within one specific neuronal system – the rodent barrel system.

The rodent barrel system processes tactile information arising from the whiskers. Incoming information from different whiskers is segregated into parallel processing lines; information from a particular whisker is delivered to a whisker-specific population of thalamocortical cells (TC cells, the encoders) within the ventral posterior medial nucleus of the thalamus. TC cell axons converge onto and weakly excite a regular spiking neuron (RS cell, the decoder) within the barrel cortex, but en route also strongly excite a population of cortical fast-spiking interneurons (FS cells, the inhibitory interneurons) which in turn supply potent, time-lagging inhibition to the RS cell decoder (Bruno 2011; Petersen 2007; Sun et al. 2006; Cruikshank et al. 2007). The major sensory feature encoded by the TC population is whisker deflection velocity, and the primary encoding variable is population synchrony; different whisker deflection velocities lead to similar net firing rates of the TC population, but higher deflection velocities yield greater synchrony among the spikes of the TC cells. Intuitively, one would expect that higher whisker deflection velocities would therefore lead to greater temporal precision of RS cell spikes (i.e., lower jitter in RS cell spike times). Interestingly, however, data show that jitter in the timing of RS cell spikes is approximately the same for all deflection velocities, but that raising deflection velocity increases the probability that the RS cell emits spikes. In other words, the synchrony code employed by the TC population is transformed into a rate code at the level of the RS cell (Temereanca et al. 2008; Pinto et al. 2000; Bruno and Sakmann 2006). Thus, the TC-FS-RS circuit provides an excellent example of phase-delayed inhibition – TC cells use population synchrony to encode deflection velocity, and the RS cell employs phase-delayed inhibition to decode TC cell synchrony.

An especially intriguing facet of the barrel system pertains to the physiological changes that occur with adaptation. If a whisker is deflected repeatedly with fixed velocity, the corresponding TC population response remains relatively unchanged, but synapses within the TC-FS-RS circuit weaken substantially. TC→RS synapses decrease in strength by 50 %, while TC→FS synapses diminish in strength by 70 % and FS→RS synapses decrease in strength to 50 % of their pre-adaptation values. Furthermore, the probability that the RS cell spikes decreases with adapta-

tion, while the jitter in the timing of RS cell spikes rises (Temereanca et al. 2008; Gabernet et al. 2005). Thus, excitation and inhibition to the RS cell both weaken, but inhibition dampens substantially more than excitation, altering the ratio of excitation to inhibition impinging upon the RS cell. Interestingly, evidence suggests that RS cell responses may actually be able to better distinguish among whisker deflection velocities following adaptation (Wang et al. 2010; Adibi et al. 2013a, b).

In this study, we construct a realistic biophysical model of the feedforward TC-FS-RS circuit, and we examine the network properties that give rise to the above experimental observations.

2 Results

To examine the encoding of whisker deflection velocity in the rodent barrel cortex, we construct a model of the feedforward TC-FS-RS circuit (Fig. 1A). We designate a population of ∼100 TC cells, and we assign a single spike to each TC cell in response to a whisker deflection (Bruno and Sakmann 2006; Bruno and Simons 2002; Pinto et al. 2000). We draw the times of TC spikes from one of four distributions: Gaussian, inverse Gaussian, exponential, or uniform, with the standard deviation of these distributions chosen to approximate experimental data for a fixed whisker deflection velocity. Though we examine all four spike time distributions, we note that the inverse Gaussian distribution best matches the experimentally observed distribution of TC spike times in response to a whisker deflection (Pinto et al. 2000). Furthermore, the model consists of 100 FS cells and a single RS neuron; the membrane potential of each FS and RS cell is governed by integrate-and-fire dynamics. We fix the network structure, with a 0.63 probability of a TC→FS synapse, and with TC and FS cells synapsing onto the RS neuron with probability 1 (Bruno and Simons 2002). Each TC spike produces a strong excitatory synaptic current in postsynaptic FS cells and a relatively weak excitatory synaptic current in the RS neuron; each FS spike elicited by TC inputs produces an inhibitory current in the RS neuron (Cruikshank et al. 2007). Due to network structure, along with a small, manually imposed synaptic delay, inhibition to the RS cell, relative to excitation, is powerful and arrives with a slight time lag. Details and experimental justification for network parameters are provided in the *Methods*.

The output of the model is the response of the RS neuron. In particular, to assess the response to a simulated fixed whisker deflection velocity, we study two features of the RS cell response: 1) the probability that the RS cell spikes (given by the number of trials during which the RS cell spikes/the total number of trials), and 2) the jitter in the timing of RS cell spikes (given by the standard deviation in the timing of the first RS cell spike, computed using trials on which the RS cell produces at least one spike). Experimentally, since whisker deflection velocity is encoded by the TC population via synchrony, rather than firing rate (i.e., increasing whisker deflection velocity produces a higher synchrony among TC cell spikes but leaves the total number of spikes unchanged) (Pinto et al. 2000; Bruno and Sakmann 2006; Temereanca et al. 2008), we simulate different whisker deflection velocities by altering the standard deviation of the TC cell spike time distribution while leaving the total number of TC cell spikes unchanged. In Fig. 2, we depict the probability that the RS cell spikes in response to various whisker deflection velocities (with different velocities simulated by modulating the synchrony of the TC population); for all four TC spike time distributions, we see concordance with experiment – as deflection velocity increases, the probability that the RS cell responds rises. This occurs as a consequence of the phase-delayed inhibition network structure; as whisker deflection velocity (i.e., TC cell synchrony) increases, temporal pooling of excitation to the RS cell creates a sharper time window within which the RS cell can respond to excitation while unopposed by time-lagging inhibition arriving from the FS cell population.

2.1 Adaptation

Repeated deflections of a whisker at a fixed velocity lead to system adaptation – synapses throughout the TC-FS-RS circuit weaken substantially. Experimentally, it is found that, after adaptation, TC to RS synaptic strengths decrease to ∼50 % of their pre-adaptation values, TC to FS synaptic strengths decrease to ∼30 % of their pre-adaptation values, and FS to RS synaptic strengths decrease to ∼50 % of their pre-adaptation values. Furthermore, the probability that the RS cell spikes decreases from ∼0.25 pre-adaptation to <0.1 post-adaptation, while the jitter in the timing of RS cell spikes increases from ∼4 ms pre-adaptation to ∼8 ms post-adaptation (Gabernet et al. 2005).

To mimic adaptation in our model, we lower TC to RS synaptic strengths to ∼30 % of the pre-adaptation value, TC to FS synaptic strengths to 31 % of the pre-adaptation value, and FS to RS synaptic strengths to 47 % of the pre-adaptation value (see *Methods* for details). For all TC spike time distributions, our model exhibits the experimentally observed decrease in spiking probability of the RS cell following adaptation (Fig. 3, left). However, we find in our model that jitter in the timing of RS cell spikes increases following adaptation only for certain distributions – we find that the inverse Gaussian, exponential, and uniform distributions all exhibit this behavior, while jitter actually shows a small decline following adaptation for the Gaussian distribution (Fig. 3, right). We note that the change in jitter (in the

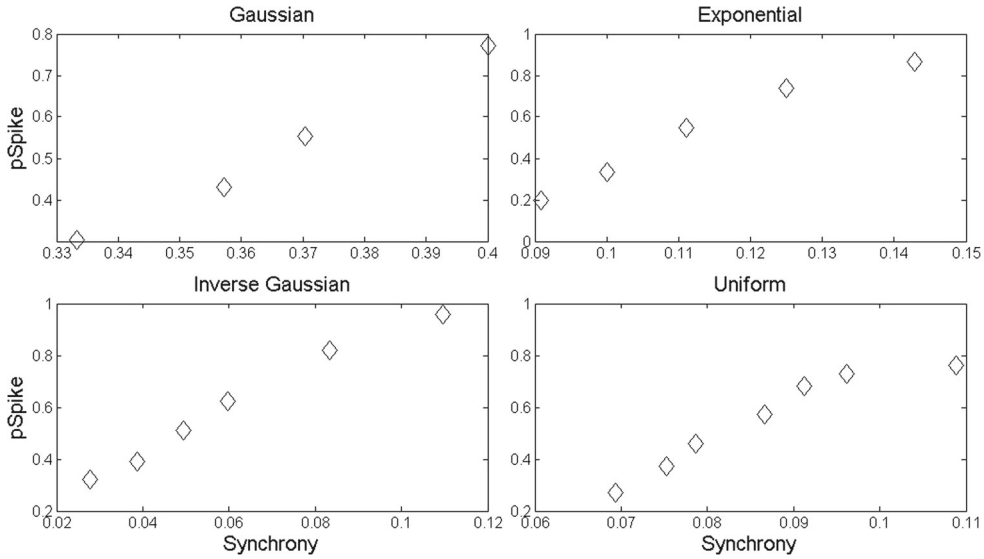

Fig. 2 Probability of response of the RS cell to different simulated whisker deflection velocities for various TC cell spike time distributions. Whisker deflection velocity is represented by TC population synchrony, where synchrony=1/standard deviation of TC spike time distribution

cases where jitter increases post-adaptation) qualitatively but not quantitatively matches the experimental data. This is a consequence of the fact that our model aims to specifically elucidate the dynamics of the feedforward phase-delayed inhibition circuit involving a single RS neuron; in the cortex, a large fraction of inputs to an RS cell originate from other cortical cells (Benshalom and White 1986), and these inputs likely supply 'noise' to the RS cell spikes induced by feedforward TC and FS cell inputs. Since our model does not account for these cortical inputs, we require only qualitative, rather than quantitative, agreement of RS cell jitter in our model with that observed in experiment.

In order to parse this behavior, we examine how our network behaves under varying strengths of TC to RS synapses. We vary the initial, pre-adaptation TC to RS synaptic strength, but we keep the percent reduction in TC to RS synaptic strength following adaptation the same as above. Furthermore, the parameters for TC to FS and FS to RS synaptic strengths pre- and post-adaptation are fixed as above. As shown in Fig. 4 (left), the probability of RS cell spiking decreases after adaptation if TC to RS synaptic strengths are weak; however, above a certain TC to RS synaptic strength, the probability of RS cell spiking actually *increases* following adaptation. Thus, to obtain experimentally consistent results in our model in terms of probability of RS spiking, pre-adaptation TC to RS synaptic strengths are required to be sufficiently weak.

This occurs because of the differential change in excitation versus inhibition to the RS cell following adaptation. Following adaptation, both excitation and inhibition to the RS cell weaken considerably, but inhibition diminishes substantially more than excitation. If TC to RS synapses are very strong pre-adaptation, then the inability of TC input to trigger spikes in the RS cell on every trial is a consequence of inhibitory suppression. Following adaptation, TC→RS synapses weaken but remain potent enough to consistently push the RS cell above threshold, and since inhibitory opposition is no longer a large factor, the RS cell fires with higher probability than in the pre-adaptation scenario. If TC→RS synapses are too feable pre-adaptation, then inhibition arriving from FS cells swamps excitation, and the RS cell cannot spike at all pre-adaptation. To obtain the experimentally observed decrease in RS cell spike probability following adaptation, TC to RS synapses must be powerful enough to consistently spark the RS cell pre-adaptation (with inhibitory suppression preventing RS

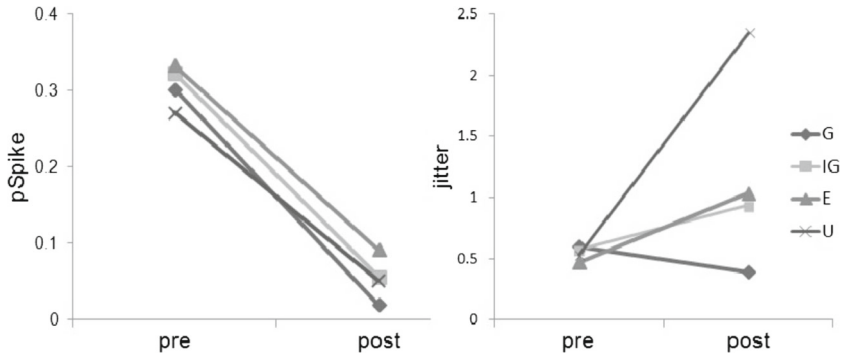

Fig. 3 Pre-adaptation and post-adaptation values for the probability that the RS cell spikes (*left*) and jitter in ms in the timing of RS cell spikes (*right*). To mimic adaptation, we lowered the strength of TC→RS, TC→FS, and FS→RS synapses to ∼30 %, 31 %, and 47 %, respectively, of their pre-adaptation values (see *Methods* for details)

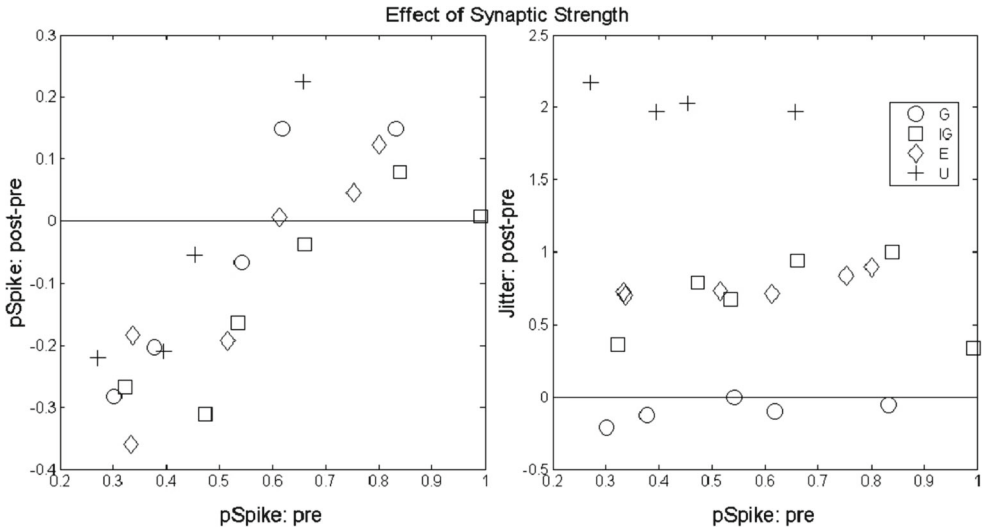

Fig. 4 Difference in post-adaptation and pre-adaptation probability of RS cell spiking (*left*) or jitter in RS cell spiking (*right*) as pre-adaptation TC to RS synaptic strength is varied. Pre-adaptation TC to FS and FS to RS synaptic strengths are fixed, and the reduction in synaptic strengths following adaptation, written as percentage of pre-adaptation values, are as follows: ∼30 % for TC to RS synapses, 31 % for TC to FS synapses, and 47 % for FS to RS synapses. The pre-adaptation probability of RS cell spiking is plotted on the abscissa as a proxy for pre-adaptation TC to RS synaptic strength

spikes on many trials), but weak enough such that, following the post-adaptation decline in strength, TC inputs often fail to provide sufficient aggregate excitation to nudge the RS cell above threshold.

In terms of RS cell spike jitter, on the other hand, we find little effect of varying the pre-adaptation TC to RS synaptic strength (Fig. 4, right). In order to illustrate the mechanism responsible for the increase in RS cell jitter following adaptation, we sever FS→RS synapses (removing inhibition to the RS cell) without altering the parameters of TC→RS synapses, and we plot the mean spike time of the RS cell (Fig. 5, left) and the jitter in RS cell spiking (Fig. 5, right) pre- and post-adaptation. Figure 5 (right) shows that, in the absence of inhibition, RS cell jitter rises in general (due to the fact that inhibition serves to curtail the effective temporal response window of the RS cell, as seen in experiment (Gabernet et al. 2005)), but we still observe a qualitatively similar increase in jitter following adaptation. Hence, inhibition is not responsible for the increase in RS cell jitter following adaptation observed in the full network – though the effective temporal response window of the RS cell imposed by inhibition increases after adaptation (since weaker TC→FS synapses lead to a higher FS spike latency), the qualitative increase in RS cell jitter can be attributed to weakened TC→RS synapses alone.

Thus, our results indicate that the effects of adaptation for a fixed whisker deflection velocity (a decrease in RS spike probability and an increase in RS cell jitter) can be explained solely by weakening of TC→RS synapses, with little dependence on the changes that occur in the parameters governing inhibition. If inhibition plays little role in adaptation, then the question naturally arises: 'what is the purpose of phase-delayed inhibition in the TC-FS-RS circuit?' We examine this question in subsequent sections.

2.2 Encoding of deflection velocity

The velocity of whisker deflections in the rat barrel cortex is encoded by the degree of synchrony of thalamic cells – higher deflection velocities lead to greater TC popula-

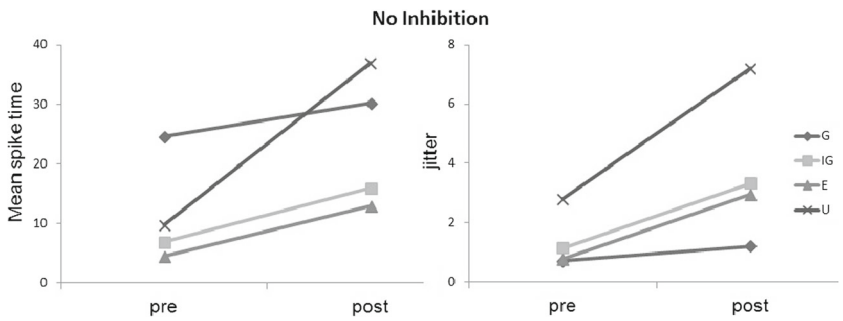

Fig. 5 Pre- and post-adaptation values for mean spike time (i.e., latency) of the RS cell in ms (*left*) and jitter in RS cell spiking in ms (*right*), in the case that FS to RS synapses are severed (i.e., no inhibition to the RS cell). Post-adaptation TC→RS synaptic strengths are lowered to ∼30 % of the pre-adaptation value

tion synchrony, while the quantity of total TC cell spikes does not change appreciably. Different levels of TC cell synchrony yield different spiking probabilities in the RS cell; higher synchrony results in an increased likelihood of RS cell spikes, while lower synchrony results in a lower probability of RS cell spiking. Jitter in RS cell spiking, however, does not seem to vary across different degrees of TC population synchrony (Temereanca et al. 2008; Pinto et al. 2000; Bruno and Sakmann 2006). Thus, the animal differentiates among various whisker deflection velocities via RS cell spiking probability.

As seen in the previous section, after adaptation, the probability of RS cell spiking decreases. Interestingly, experiments suggest that RS cell spiking may be better able to distinguish among whisker deflection velocities post-adaptation, while the higher level of RS cell spiking pre-adaptation may provide more reliable information about whether or not a deflection has occurred (Wang et al. 2010; Adibi et al. 2013a, b). In this section, we examine the pre-adaptation to post-adaptation change in the sensitivity of RS cell spiking probability to whisker deflection velocity in our model. We simulate different deflection velocities by modulating the standard deviation of the distribution of TC cell spike times (↑deflection velocity=↓standard deviation).

In Fig. 6, we depict the probability (top panels) and jitter (bottom panels) of RS cell spikes in response to varying whisker deflection velocities, both pre- and post-adaptation. In the top panels, the slopes (denoted by m) of the best fit lines indicate the sensitivity of RS cell responses to TC population synchrony – the larger the slope, the greater the ability of RS cell spikes to differentiate among deflection velocities. Figure 6 (top panels) shows that RS cell spiking probability increases with TC population synchrony, and that for the inverse Gaussian and the uniform TC spike time distributions, sensitivity to TC synchrony increases following adaptation ($m = 8.0908$ pre- and $m = 11.239$ post-adaptation for inverse Gaussian; $m = 15.786$ pre- and $m = 30.99$ post-adaptation for uniform). However, for the exponential distribution, the sensitivities pre- and post-adaptation are similar ($m = 14.01$ pre- and $m = 13.188$ post-adaptation), while for the Gaussian distribution, the slope diminishes slightly following adaptation ($m = 7.1551$ pre- and $m = 5.3068$ post-adaptation). Moreover, jitter remains relatively constant across varying levels of TC population synchrony for all distributions. Thus, for all TC spike time distributions, our model captures the experimental data on RS cell responses (increasing spiking probability and invariance of jitter in relation to TC synchrony), while an increased sensitivity of RS cell spiking to TC population synchrony following adaptation is seen only for the inverse Gaussian and uniform distributions.

In Fig. 7, we carry out the same analysis as in Fig. 6, except we remove inhibition from our model (i.e., only TC→RS synapses remain). In the absence of inhibition, the RS cell spikes with probability 1 pre-adaptation, for all TC spike time distributions and synchrony levels. Post-adaptation, the RS cell is substantially less sensitive to TC population synchrony than in the presence of inhibition (slopes: $m = 6.8704$ for inverse Gaussian, $m = 1.9222$ for Gaussian, $m = 2.8894$ for exponential, $m = 6.5048$ for uniform). The sensitivity of the RS cell to TC synchrony, both pre- and post-adaptation, is substantially less without inhibition (Fig. 7) than with intact inhibitory synapses (Fig. 6).

To obtain better pre- and post-adaptation comparisons in the absence of inhibition, we adjust the TC→RS synaptic strength such that $P(\text{RS cell spikes}) < 1$ pre-adaptation. In particular, we lower the pre-adaptation TC to RS synaptic strength such that, even at the highest TC synchrony level, the probability of RS cell spiking is below 1 (see *Methods* for details). The post-adaptation TC→RS synaptic strength is set at ∼90 % of its pre-adaptation value (a lower post-adaptation strength results in the RS cell failing to produce any spikes following adaptation). The results are shown in Fig. 8; the slopes of the best fit lines for $P(\text{RS cell spikes})$, pre- and post-adaptation, are as follows: $m = 3.5212$ pre and $m = 8.2596$ post (inverse Gaussian), $m = -0.0911$ pre and $m = 1.5315$ post (Gaussian), $m = 8.1843$ pre and $m = 7.3446$ post (exponential), $m = 14.501$ pre and $m = 20.464$ post (uniform). In this scenario, we again see that the sensitivity of RS cell spiking to TC population synchrony in the absence of inhibition (Fig. 8), both pre- and post-adaptation, is considerably worse than in the case that the RS cell utilizes a phase-delayed inhibition decoding scheme (Fig. 6).

Hence, we conclude that phase-delayed inhibition enhances the sensitivity of RS cell spiking to TC population synchrony – sensitivity declines markedly when inhibitory synapses are severed in our model (i.e., when the RS cell acts purely as a high spike threshold synchrony decoder). Even a minimal presence of phase-delayed inhibition is sufficient to substantially augment RS cell sensitivity. In the full network (Fig. 6), inhibition dampens more than excitation post-adaptation (causing inhibition to be reduced to a low level), while in Fig. 7, post-adaptation parameters are identical, except that the network completely lacks inhibition. Despite the presence of only a modest amount of inhibition in the full network post-adaptation, RS cell sensitivity is still considerably higher than in the complete absence of inhibition.

Thus, phase-delayed inhibition is needed to construct an RS cell decoder with maximal ability to distinguish among whisker deflection velocities. However, this poses an interesting question in light of adaptation dynamics. Following adaptation, inhibitory synapses weaken substantially more than excitatory synapses, increasing the ratio of excitation

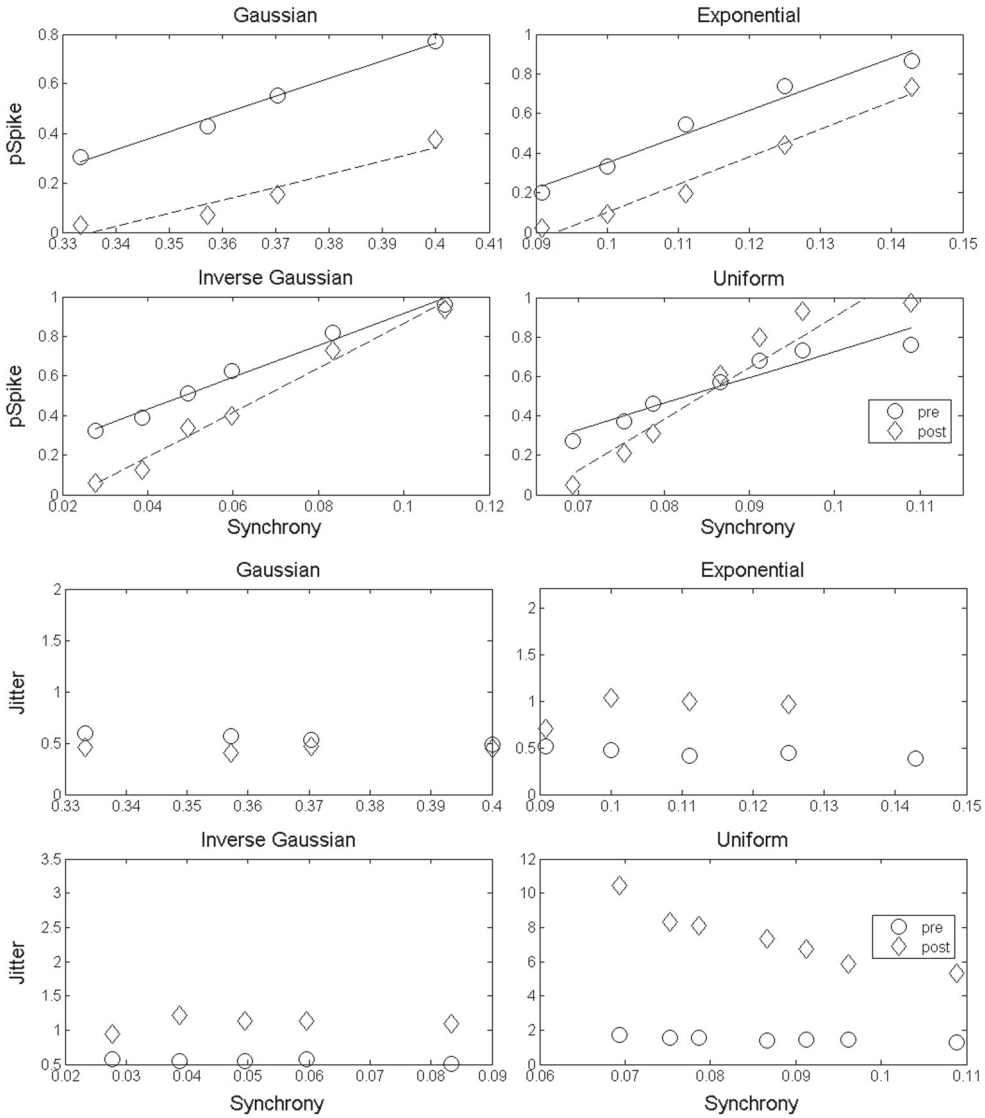

Fig. 6 Probability that the RS cell spikes (*top panels*) and jitter in ms in RS cell spikes (*bottom panels*) pre- and post-adaptation, in response to varying levels of TC population synchrony (synchrony=1/standard deviation of TC spike time distribution). Network parameters other than the standard deviation of the TC spike time distribution are fixed at their standard pre- and post-adaptation values (see *Methods* for details). The slopes (m) of the best fit lines in the probability of RS cell spiking plots, pre-adaptation and post-adaptation, are as follows: $m = 8.0908$ pre and $m = 11.239$ post (inverse Gaussian), $m = 7.1551$ pre and $m = 5.3068$ post (Gaussian), $m = 14.01$ pre and $m = 13.188$ post (exponential), $m = 15.786$ pre and $m = 30.99$ post (uniform)

to inhibition impinging upon the RS cell decoder. Why does the ratio of excitation to inhibition change post-adaptation? Why not proportionally dampen excitation and inhibition?

2.3 Dynamics of phase-delayed inhibition

The answer to this question harkens back to our prior work on the dynamics of the phase-delayed inhibition network structure (Patel and Joshi 2013; Joshi and Patel 2013). In this earlier work, we show that the synchrony detection properties of a decoder employing phase-delayed inhibition depend only on the ratio of net excitation to net inhibition impinging upon the decoder – so long as this ratio remains fixed, the ability of the decoder to decipher synchrony is invariant to changes in the number, strength, or time scale of excitatory and inhibitory synaptic inputs. In particular, proportional modifications in the amplitudes of incoming excitatory and inhibitory spikes leave the ability of the decoder to discriminate among synchrony-encoded stimuli unchanged. Within the specific context of the barrel system, our prior work suggests that weakening excitation and inhibition proportionally following adaptation should yield little change in the ability of the RS cell to distinguish among whisker deflection velocities.

For comparison with physiologically observed adaptation dynamics (shown in Fig. 6), we construct two artificial post-adaptation schemes. In the first scheme (lowered scheme), we proportionally diminish TC→RS and FS→RS synaptic strengths, while TC→FS synapses remain unchanged. We set TC→RS and FS→RS synaptic strengths to 90 % of their pre-adaptation values (further proportional reductions lead to an inability of the RS cell to emit any spikes). In the second scheme (raised scheme), we proportionally raise TC→RS and FS→RS synaptic strengths (while TC→FS synapses remain unaltered). TC→RS and FS→RS synaptic strengths are increased to 110 % of their

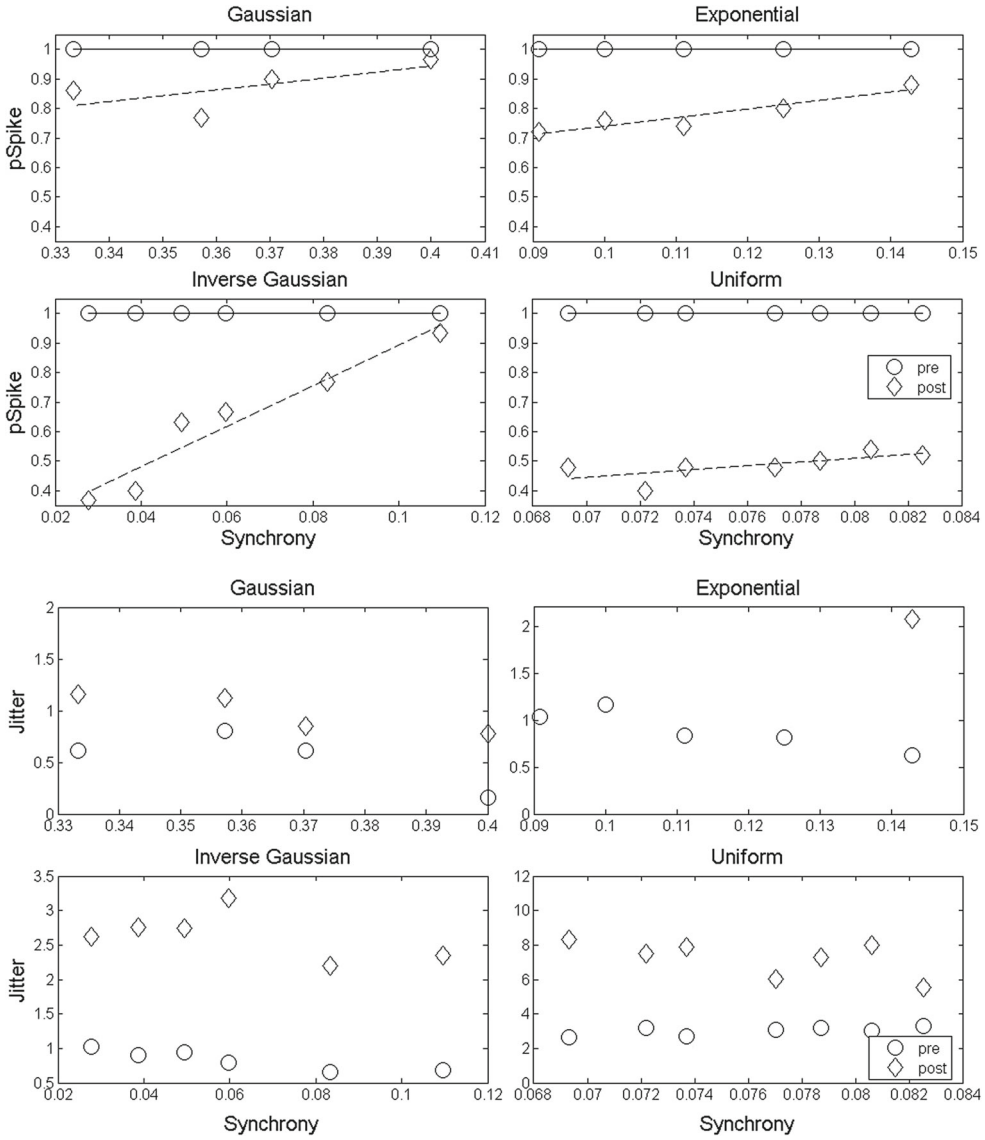

Fig. 7 Probability that the RS cell spikes (*top panels*) and jitter in ms in RS cell spikes (*bottom panels*) pre- and post-adaptation, in response to varying levels of TC population synchrony (synchrony=1/standard deviation of TC spike time distribution). Inhibition is removed from the model, and network parameters other than the standard deviation of the TC spike time distribution are fixed at their standard pre- and post-adaptation values (see *Methods* for details). Pre-adaptation, the RS cell spikes with probability 1 for all TC population synchrony levels. The slopes (m) of the post-adaptation best fit lines in the probability of RS cell spiking plots are as follows: $m = 6.8704$ (inverse Gaussian), $m = 1.9222$ (Gaussian), $m = 2.8894$ (exponential), $m = 6.5048$ (uniform)

pre-adaptation values (further proportional elevations result in saturation of the RS cell response).

In Fig. 9, we plot P(RS cell spikes) vs TC population synchrony, and we compare the ability of the RS cell to distinguish among whisker deflection velocities pre- and post-adaptation, for both artificial post-adaptation schemes. As suggested by our prior work (Patel and Joshi 2013; Joshi and Patel 2013), the ability of the RS cell to distinguish among different levels of TC population synchrony exhibits little change pre- to post-adaptation for both the lowered and raised schemes (the best fit lines pre- and post-adaptation exhibit similar slopes). This occurs as a consequence of the fact that the only change post-adaptation is a proportional modulation in the amplitude of excitatory and inhibitory synaptic inputs to the RS cell; since the ratio of excitation to inhibition delivered to the RS cell remains fixed, the synchrony detection properties of the RS cell do not change.

We therefore propose that the alteration in the sensitivity of the RS cell to whisker deflection velocity after adaptation is not a consequence of changes in the dynamics of inhibitory or excitatory synapses *per se*, but rather due to a change in the *ratio* of excitation and inhibition that the RS cell receives – proportional changes in excitation and inhibition have little effect on synchrony detection. From our earlier work (Patel and Joshi 2013; Joshi and Patel 2013), there are several ways to modulate the ratio of excitation to inhibition delivered to a decoder and hence alter its synchrony detection properties: differential modification of 1) the amplitude of excitatory and inhibitory synaptic inputs, 2) the time course of excitatory and inhibitory synaptic inputs, or 3) the number of excitatory and inhibitory input spikes. Following adaptation in the barrel system, TC→RS and FS→RS synapses diminish in potency to an approximately equal degree, and the temporal dynamics of TC

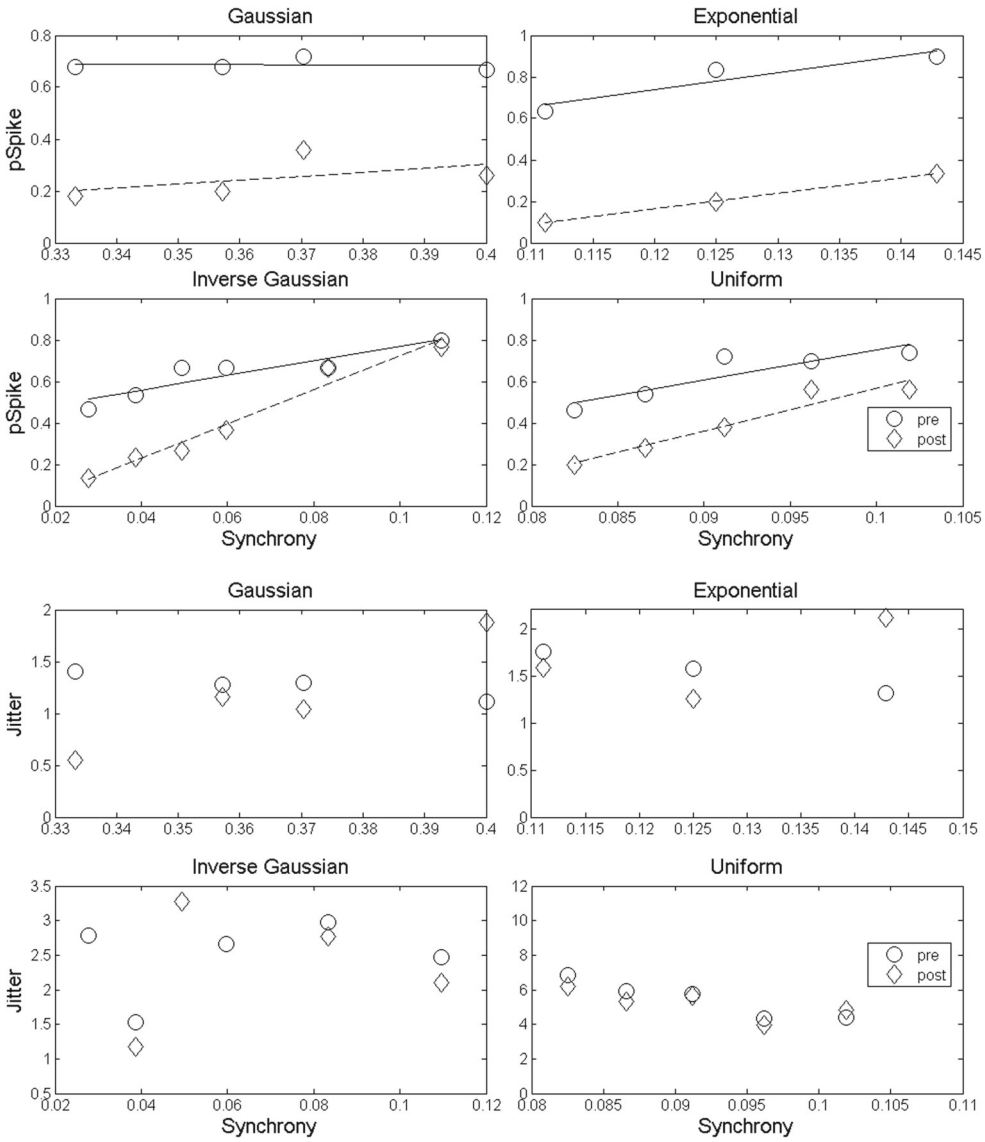

Fig. 8 Probability that the RS cell spikes (*top panels*) and jitter in ms in RS cell spikes (*bottom panels*) pre- and post-adaptation, in response to varying levels of TC population synchrony (synchrony=1/standard deviation of TC spike time distribution). Inhibition is removed from the model, and TC→RS synapses are weakened to ensure $P(\text{RS cell spikes}) < 1$ pre-adaptation. Post-adaptation TC→RS synaptic strength is set at 90 % of the pre-adaptation value (lower post-adaptation strengths lead to the RS cell not spiking following adaptation). The slopes (m) of the best fit lines in the probability of RS cell spiking plots, pre-adaptation and post-adaptation, are as follows: $m = 3.5212$ pre and $m = 8.2596$ post (inverse Gaussian), $m = -0.0911$ pre and $m = 1.5315$ post (Gaussian), $m = 8.1843$ pre and $m = 7.3446$ post (exponential), $m = 14.501$ pre and $m = 20.464$ post (uniform)

and FS inputs to the RS cell remain unchanged (Gabernet et al. 2005). Thus, the alteration in the ratio of excitation to inhibition impinging upon the RS cell is primarily due to a differential change in the number of TC and FS spikes delivered to the RS cell – the number of TC spikes does not change appreciably following adaptation, but the number of FS spikes dwindles as a consequence of TC→FS synapses diminishing considerably in strength (Gabernet et al. 2005; Pinto et al. 2000).

Furthermore, it is important to mention that there is an additional potential source of complexity in the post-adaptation dynamics of the RS cell. We note that in Fig. 7, in which inhibition is eliminated from the network but TC→RS synapses are left unmodified, the probability that the RS cell spikes is less than 1 post-adaptation. This indicates that TC→RS synapses, following adaptation, have weakened to the point that the RS cell may be able to behave like a high spike threshold detector, and hence, in the presence of phase-delayed inhibition, the RS cell may act like a mixed high spike threshold/phase-delayed inhibition decoder. However, in our model, we weaken TC→RS synapses following adaptation somewhat more than is observed biologically, so it is possible that in the actual barrel cortex, an RS cell is unable to perform high spike threshold synchrony detection even after adaptation. Regardless, the possibility of a high spike threshold component to post-adaptation RS cell dynamics would have little physiological impact. A high spike threshold mechanism essentially imposes a minimum on the level of encoder (TC cell) synchrony required to elicit a response in the decoder (RS cell), but can impart little sensitivity to the decoder in terms of fine discrimination among different encoder synchrony levels (Figs. 7 and 8; compare with Fig. 6). As long as encoder synchrony exceeds this minimum level, the

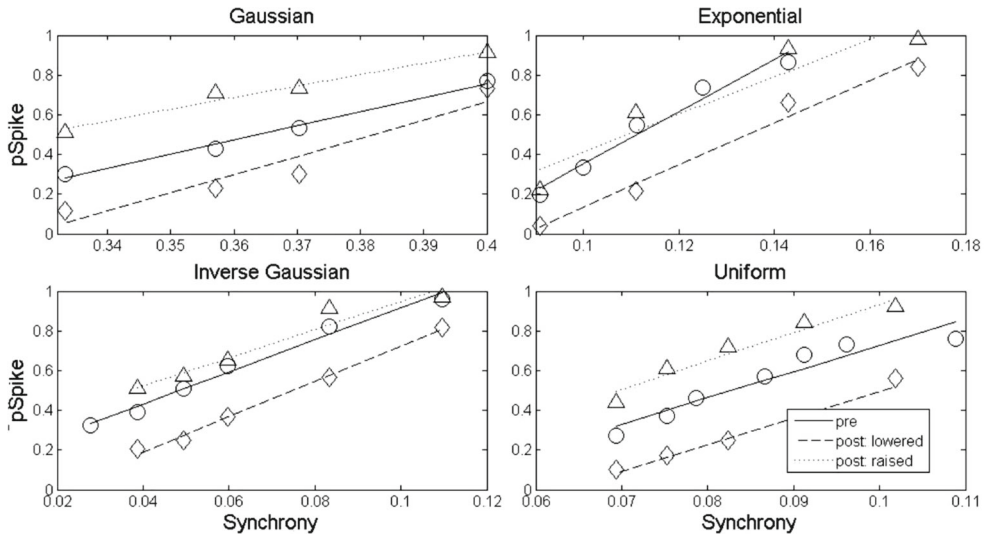

Fig. 9 P(RS cell spikes) vs TC population synchrony (synchrony=1/standard deviation of TC spike time distribution), pre-adaptation and post-adaptation, in the case that excitation and inhibition change proportionally after adaptation. We employ two post-adaptation schemes: 1) lowered scheme – TC→RS and FS→RS synaptic strengths are lowered to 90 % of pre-adaptation values, while TC→FS synaptic strength remains at its pre-adaptation value; 2) raised scheme – TC→RS and FS→RS synaptic strengths are raised to 110 % of pre-adaptation values, while TC→FS synaptic strength remains at its pre-adaptation value. The slopes (m) of the best fit lines, pre- and post-adaptation, are as follows: $m = 8.0948$ pre, $m = 8.8727$ post lowered, $m = 7.0625$ post raised (inverse Gaussian); $m = 7.1113$ pre, $m = 9.1915$ post lowered, $m = 5.7937$ post raised (Gaussian); $m = 13.1762$ pre, $m = 10.6402$ post lowered, $m = 9.4924$ post raised (exponential); $m = 13.2433$ pre, $m = 13.3088$ post lowered, $m = 14.2793$ post raised (uniform)

high spike threshold mechanism has little practical effect on decoder dynamics, and the phase-delayed inhibition mechanism is the source of the decoder's ability to robustly distinguish various degrees of encoder synchrony (Patel and Joshi 2013; Joshi and Patel 2013).

3 Discussion

In this work, we extend our prior work (Patel and Joshi 2013; Joshi and Patel 2013), in which we examine the dynamics of the phase-delayed inhibition network architecture in general, to the specific setting of the rodent barrel cortex, in which cortical RS cells employ phase-delayed inhibition to decipher whisker deflection velocity encoded via TC population synchrony. We construct a biological model of the feedforward TC-FS-RS circuit, and we show that our model captures the experimentally observed properties of RS cell responses in terms of adaptation dynamics and encoding of whisker deflection velocity. Moreover, we show that, when considering a fixed whisker deflection velocity, system adaptation to repeated whisker deflections can be explained solely by dynamical changes in TC→RS excitation, without any need to appeal to phase-delayed inhibition. However, we find that phase-delayed inhibition is crucial in allowing the RS cell to distinguish among whisker deflection velocities, and to capture the changes in the ability of the RS cell to discriminate synchrony-encoded stimuli following adaptation. In particular, we postulate that the key property that explains the changing sensitivity of the RS cell pre- to post-adaptation is the change in the *ratio* of excitation to inhibition impinging upon the RS cell.

3.1 TC spike time distributions

In our investigations, we employ 4 different TC spike time distributions: inverse Gaussian, Gaussian, exponential, and uniform. While the majority of our results do not depend on the specific distribution employed, it is important to mention that some of our results do exhibit qualitative differences among distributions. For the Gaussian distribution, jitter in RS cell spiking decreases following adaptation, in constrast to the other distributions (Fig. 3); in the absence of inhibition (Fig. 5), though, the Gaussian yields qualitatively similar behavior to the other distributions, indicating that inhibition is responsible for causing the decline in RS cell jitter after adaptation seen with the Gaussian distribution (we surmise that this is related to the fact that the Gaussian is the only distribution with a significant 'left tail'). In terms of sensitivity of the RS cell to TC population synchrony, we see in Fig. 6 that for the Gaussian and exponential distributions, the ability of the RS cell to discriminate among whisker deflection velocities actually declines somewhat following adaptation, in contrast to the

other distributions. It is intriguing to note that the basic behavior of our model can exhibit some variation for qualitatively different TC spike time distributions, and this provides an interesting avenue for future detailed explorations. For the purposes of the present study, however, we note that the inverse Gaussian best models the shape of the experimentally observed distribution of TC spike times (Pinto et al. 2000), and in our model inverse Gaussian-distributed TC spike times yield results concordant with experiment in all tests.

3.2 Extensions of our model

Our model examines the feedforward circuit consisting of a population of whisker-specific TC cells, a population of FS cells, and a single RS neuron, and we show that this circuit is able to qualitatively, and often quantitatively, capture the experimentally observed properties of the RS cell response to whisker deflection velocity and adaptation. However, our model only examines the dynamics of a single component, a basic 'building block', of the entire barreloid/barrel cortex network. For a given whisker, there are ∼250 TC cells, ∼400 FS cells, and ∼3600 RS cells in the barrel system corresponding to that whisker, and each RS cell in a barrel receives input from ∼90 TC cells and some subset of the FS cells (Bruno and Simons 2002). Thus, for a given whisker, there are actually multiple parallel and overlapping feedforward TC-FS-RS cell circuits. Furthermore, RS cell responses within a barrel are direction-specific (whisker-specific RS cells can be split into subpopulations that each have a preferred direction of whisker deflection) (Wilent and Contreras 2005; Bruno and Sakmann 2006), and the majority of inputs to an RS cell originate from other cortical (FS and RS) cells rather than from TC cells (Benshalom and White 1986). Finally, there is a massive amount of corticothalamic feedback, which may exert both excitatory and inhibitory effects on the TC population (Temereanca and Simons 2004; Guillery 1967; Liu et al. 1995). In future work, our basic TC-FS-RS model can be used as a 'building block' to construct a large-scale model of a single barreloid/barrel system. A large-scale model would consist of a population of whisker-specific TC, FS, and RS cells, with different RS cells receiving feedforward input from different (but overlapping) subsets of TC and FS cells, and with lateral connections between RS cells. Such a model can be used to study the emergence of direction selectivity, and further extensions of the model can be used to study the dynamical interactions between different whisker-specific barrels. Additionally, another interesting avenue that such large-scale modeling can be used to explore is the role of corticothalamic feedback, whose role in the barrel system (and in the thalamocortical system in general) is as of yet largely unknown.

3.3 Function of adaptation

Following adaptation, RS cell spiking diminishes while the sensitivity of RS cell responses to whisker deflection velocity increases, and it has been postulated that the role of adaptation dynamics may be to ensure that, pre-adaptation, the animal is able to robustly detect the occurrence of a whisker deflection (due to a high level of RS cell spiking). After adaptation, it is less important for the animal to determine whether or not a deflection has occurred (since, after repeated deflections, the animal is presumably aware that a deflection has occurred) and the increased sensitivity of RS cells responses allows the animal to precisely discriminate among different whisker deflection velocities (Gabernet et al. 2005; Wang et al. 2010; Adibi et al. 2013a, b). Additionally, decreased RS cell spiking allows allocation of a smaller fraction of the limited neuronal resources available to the animal to the processing of ongoing whisker deflections.

A particularly interesting possibility is that adaptation plays a role in the dynamics of whisker-whisker interactions. In natural roaming activity, it is probable that multiple whiskers are deflected repeatedly and simultaneously, which implies that, in natural settings, multiple barrels within somatosensory cortex are likely to be active concurrently and in various states of adaptation. Adaptation, therefore, may serve to shape the functional interplay among different whisker barrels, molding activity patterns across somatosensory cortex and pinpointing novel deflection information that can guide moment-to-moment reallocations of attentional or processing resources. This will be explored in future modeling work.

3.4 Other models

There have been several prior modeling studies within the barrel system aimed at elucidating cortical dynamics. In Pesavento et al. (2010) and Pesavento and Pinto (2012), the authors employ a hybrid experimental/simulation approach to explore the detailed response properties of individual barrel neurons within the context of thalamic and cortical inputs, and the authors delineate the precise interplay of synaptic input and intrinsic neuronal properties that give rise to the dynamical behavior of an FS or RS neuron. In Pinto et al. (2003), the investigators examine the effect of thalamic synchrony on cortical cell responses and the transformation of neuronal receptive fields from thalamic to barrel cells, as well as describe a net damping effect of corticocortical interactions. In Kyriazi and Simons (1993), the investigators construct a biophysical integrate-and-fire model of barrel cortex and study the net effects of spatial and temporal integration within a barrel, and in Pinto et al. (1996) the authors course-grain this integrate-and-fire model in order

to develop a population model of barrel cortex capable of both qualitative and quantitative predictions. In Ly et al. (2012) and Middleton et al. (2012), the authors use modeling approaches to examine variability in the responses of barrel cortical neurons and study the role of feedforward inhibition in maintaining low correlations in excitatory cortical populations.

Our work differs from prior work in that we focus specifically on a single feedforward 'building block' of the cortical barrel circuit, and the dynamics of its phase-delayed inhibition synchrony detection scheme. In terms of modeling philosophy, our work follows a similar approach to Kyriazi and Simons (1993), in that we do not attempt to incorporate the detailed intrinsic neuronal properties of TC, FS, and RS cells; rather, we construct a biophysically-oriented model that captures the network structure and dynamics of our object of interest. Moreover, we specifically study the contribution of a single phase-delayed inhibition TC-FS-RS 'building block' to the ability of an RS cell to discriminate whisker deflection velocity and give rise to adaptation dynamics, a perspective which, to our knowledge, has not been explored in prior work. The advantage of our approach is the ability to distill the component of RS cell encoding behavior produced by purely feedforward phase-delayed inhibition circuitry; further large-scale modeling work that expands upon our 'building block' model, and incorporates intracortical connectivity within and across barrels, may benefit from the explicit delineation of phase-delayed inhibition dynamics laid out in this study.

4 Methods

In this study, we construct a model of the feedforward circuit consisting of a whisker-specific TC population, a set of inhibitory FS cells driven by the TC neurons, and a single RS cell that receives input from the TC and FS populations.

Experimental observations indicate that an RS cell receives convergent input from ∼90 TC cells (Bruno and Sakmann 2006; Bruno and Simons 2002), and that whisker deflections tend to elicit ∼1 spike in each TC cell (Pinto et al. 2000). Accordingly, the number of TC cell spikes in our model in response to a whisker deflection is drawn from a Gaussian distribution with mean 100 and standard deviation 3. TC cells are not explicitly modeled; the times of the TC cell spikes are independently drawn from one of four distributions: Gaussian, inverse Gaussian, exponential, or uniform. We note that of the four distributions we employed, the inverse Gaussian is the most concordant with experimentally measured TC spike time distributions (Pinto et al. 2000). Standard parameters for these distributions, chosen to approximate experimental data for a fixed whisker deflection velocity (Pinto et al. 2000), are as follows: Gaussian had mean 25ms and standard deviation 3ms, inverse Gaussian had mean 10 ms and standard deviation 9.13 ms, exponential had mean 10ms, and uniform had mean 25 ms and standard deviation 14.4 ms (Fig. 10).

The model also consists of 100 FS cells and a single RS neuron, with a 0.63 probability of synapse from a TC cell onto an FS cell, in accordance with experiment (Bruno and Simons 2002). All TC and FS cells synapse onto the single RS neuron.

The membrane potential of each FS/RS cell is governed by a reduced dimensional integrate-and-fire model:

$$\frac{dV_j^k}{dt} = -gV_j^k + I_j^k(t), \tag{1}$$

where $k \in \{\text{FS,RS}\}$, while $j \in \{1,2,...,100\}$ for $k = \text{FS}$ and $j \in \{1\}$ for $k = \text{RS}$. V_j^k is the non-dimensional membrane potential, $g = 0.05\ \text{ms}^{-1}$ is the leak conductance, and $I_j^k(t)$ is the synaptic current (in ms^{-1}). $V_o = 0$ is the resting potential, and a spike is recorded when $V_j^k \to 1^-$, at which point V_j^k is instantaneously reset to V_o. A refractory period is simulated by holding V_j^k at V_o for 2 ms following a spike. We note that the model has a membrane time constant of 20 ms, consistent with the experimentally observed ∼17 ms time constant of RS cells (Gabernet et al. 2005). Details of the reduced dimensional model are given in Tao et al. (2004).

Every time a TC cell spike occurs, a synaptic input is sent to the RS cell and to postsynaptic FS cells. Each FS cell spike elicits a synaptic current in the RS cell, with a manually imposed 0.5 ms synaptic delay. Synaptic inputs to neuron k, j are modeled through the $I_j^k(t)$ term. Let n_j^k denote the total number of presynaptic spikes impinging upon neuron k, j. If the r^{th} presynaptic spike occurs at time $t_{j,r}^k$, the current induced in neuron k, j is given by the following:

$$i_{j,r}^k(t) = \begin{cases} 0 & t < t_{j,r}^k + d, \\ Ae^{-\alpha(t-t_{j,r}^k-d)} & t \geq t_{j,r}^k + d. \end{cases} \tag{2}$$

$$I_j^k(t) = \sum_{r=1}^{n_j^k} i_{j,r}^k(t). \tag{3}$$

A indicates the strength of the input, α dictates the decay rate, and d denotes the synaptic delay. For the synaptic delay, we set $d = 0$ for TC→FS and TC→RS synapses, and $d = 0.5$ for FS→RS synapses. We introduced the delay parameter to match the experimental observation that TC spikes lead to an EPSP in the RS cell followed by an IPSP with a 1-2 ms time lag (Gabernet et al. 2005). For the decay rate, we set $\alpha = 0.7324$ for TC to FS synapses, $\alpha = 0.2441$ for TC to RS synapses, and $\alpha = 0.1772$ for FS to RS synapses. We chose these values to match experimental data

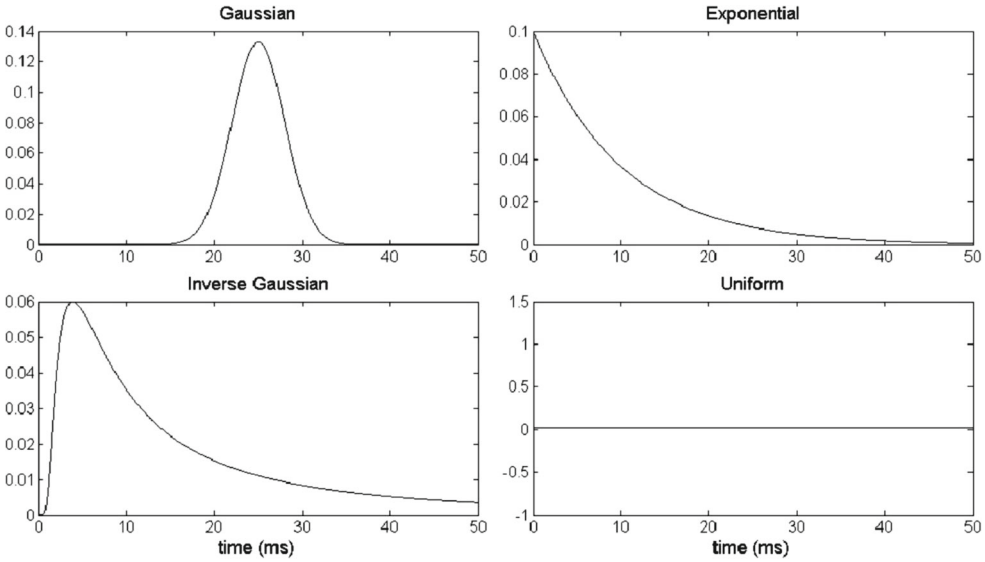

Fig. 10 Distributions from which TC cell spike times are drawn

showing that TC to FS synaptic inputs decay over a ∼1.5 ms time scale, TC to RS synaptic inputs decay over a ∼4.5 ms time scale, while FS to RS synaptic inputs decay over a ∼6.5 ms time scale (Gabernet et al. 2005).

We chose values for A in Eq. (2) such that ∼10 incoming TC spikes are sufficient to trigger a spike in an FS cell, and ∼30-40 incoming TC spikes are required to elicit a spike in the RS cell (Temereanca et al. 2008). We set $A = 0.3$ for TC to FS cell synapses and $A = -0.003$ for FS to RS synapses. TC→FS synapses are mildly weaker in our model than observed empirically (experiments show that one or a few TC spikes are sufficient to elicit a spike in an FS cell (Gabernet et al. 2005)); this is because, in our model, we do not account for inhibitory synapses among FS cells (Cruikshank et al. 2007), and we possibly overestimate the number of FS cells converging onto a single RS cell, and hence fixing a reduced TC→FS synaptic strength prevents an unrealistically overwhelming amount of inhibition. However, our model retains the key feature of TC-FS dynamics – TC spikes reliably lead to FS spikes with a small delay. For TC to RS synapses, the exact value of A is varied slightly for the different TC spike time distributions to ensure that the RS neuron exhibits a ∼0.3 probability of spiking: $A = 0.0455$ for Gaussian, $A = 0.05$ for inverse Gaussian, $A = 0.0465$ for exponential, and $A = 0.068$ for uniform. We chose these parameters to obtain RS cell spiking probabilities consistent with experiment (Gabernet et al. 2005), as well as to agree with experimental data showing that 1) TC spikes elicit a ∼4-8 fold larger EPSP in an FS cell than in an RS cell (Cruikshank et al. 2007) and 2) the postsynaptic current in an RS cell induced by a whisker deflection is dominated by inhibition (experiments show that in an RS cell the ratio $\frac{\text{EPSC}}{\text{EPSC+IPSC}} =\sim 0.2$ Gabernet et al. 2005).

For a fixed parameter regime, we obtained data from a block of 100 trials. The outputs of the model are the probability that the RS cell spikes (given by the number of trials during which the RS cell spikes/total number of trials) and the jitter in the timing of RS cell spikes (given by the standard deviation in the timing of the first RS cell spike, computed over 100 trials in which the RS cell spiked at least once). Simulations were carried out using Euler's method with a time step of 0.01 ms.

4.1 Adaptation

Repeatedly deflecting a whisker with a fixed deflection velocity leads to adaptation – synaptic strengths throughout the TC-FS-RS circuit decrease in strength: TC→RS synapses decrease in strength by ∼50 %, TC→FS synapses decrease in strength by ∼70 %, and FS→RS synapses decrease in strength by ∼50 %. This leads to a 50 % reduction in net excitation to the RS cell and a 90 % reduction in net inhibition to the RS cell (Gabernet et al. 2005). To mimic adaptation, we lower synaptic strengths (the A parameter described above) in our model in accordance with the experimentally observed synaptic strength and RS cell spiking probability changes that occur after adaptation. For all distributions, the post-adaptation strength for TC to FS cell synapses is set to 31 % of its standard value, while the post-adaptation strength for FS to RS synapses is set to 47 % of its standard value. The change in the synaptic strength A after adaptation for TC to RS cell synapses (written as percentage of its standard, pre-adaptation strength) is varied slightly across different TC spike time distributions: 26.5 % for Gaussian, 30.2 % for inverse Gaussian, 31.2 % for exponential, 26.0 % for uni-

form. To mimic adaptation, the TC to RS synaptic strength reductions are distribution-specific and somewhat greater in our model than observed experimentally; we did this in order to ensure a ∼0.1 spiking probability for the RS cell post-adaptation, in accordance with experiment. However, setting the TC to RS synaptic strength reduction post-adaptation to a value closer to that observed experimentally (50 %) yields similar qualitative behavior of our model.

4.2 Velocity

Within a whisker-specific TC cell population, different whisker deflection velocities lead to similar net spike counts within the population; however, the synchrony of TC cell spikes varies directly with deflection velocity (Pinto et al. 2000; Bruno and Sakmann 2006; Temereanca et al. 2008). To simulate the experimentally observed encoding of whisker deflection velocity by TC cell synchrony (rather than response magnitude), we simulate higher (lower) whisker deflection velocities by decreasing (increasing) the standard deviation of the TC spike time distribution in our model, while leaving the number of TC spikes unchanged.

In one set of trials in which we explore encoding of whisker deflection velocity, we remove inhibition from the system, and to compensate for the lack of inhibition we adjust TC to RS synaptic strengths to ensure that the RS cell displays a probability of spiking that is less than 1. We chose TC to RS synaptic strengths such that, even at the highest whisker deflection velocity (i.e., the highest level of TC cell synchrony), the spiking probability of the RS cell is below 1 and roughly the same as the spiking probability of the RS cell with inhibition at this level of TC cell synchrony. In addition, to mimic adaptation in this scenario, we lower the TC to RS synaptic strength A, but less so than described in the *Adaptation* section (otherwise the RS cell would not spike post-adaptation). We chose the post-adaptation value of A to obtain the post-adaptation spiking probability of the RS cell observed with inhibition (at the highest level of TC cell synchrony). The adjusted values for pre-adaptation TC to RS synaptic strengths and post-adaptation strengths (written as a percentage of pre-adaptation values) are as follows: $A = 0.005$ and 92 % for Gaussian, $A = 0.015$ and 90 % for inverse Gaussian, $A = 0.011$ and 90 % for exponential, $A = 0.016$ and 90 % for uniform.

Acknowledgments Runjing Liu and Mainak Patel were partially supported by a National Science Foundation grant (DMS-0943760).

Conflict of interest The authors declare that they have no conflict of interest.

References

Adibi, M., Clifford, C., Arabzadeh, E. (2013a). Informational basis of sensory adaptation: entropy and single-spike efficiency in rat barrel cortex. *The Journal of Neuroscience*, *33*(37), 14921–14926.

Adibi, M., McDonald, J., Clifford, C., Arabzadeh, E. (2013b). Adaptation improves neural coding efficiency despite increasing correlations in variability. *The Journal of Neuroscience*, *33*(5), 2108–2120.

Benowitz, L.I., & Karten, H.J. (2004). Organization of the tectofugal visual pathway in the pigeon: A retrograde transport study. *The Journal of Comparative Neurology*, *167*(4), 503–520.

Benshalom, G., & White, E. (1986). Quantification of thalamocortical synapses with spiny stellate neurons in layer iv of mouse somatosensory cortex. *Journal of Computational Neuroscience*, *253*(3), 303–314.

Blitz, D.M., & Regehr, W.G. (2005). Timing and specificity of feed-forward inhibition within the LGN. *Neuron*, *45*(6), 917–928.

Bruno, R. (2011). Synchrony in sensation. *Current Opinion in Neurobiology*, *21*(5), 701–708.

Bruno, R., & Sakmann, B. (2006). Cortex is driven by weak but synchronously active thalamocortical synapses. *Science*, *312*(5780), 1622–1627.

Bruno, R., & Simons, D. (2002). Feedforward mechanisms of excitatory and inhibitory cortical receptive fields. *The Journal of Neuroscience*, *22*(24), 10966–10975.

Cruikshank, S., Lewis, T., Connors, B. (2007). Synaptic basis for intense thalamocortical activation of feedforward inhibitory cells in neocortex. *Nature Neuroscience*, *10*, 462–468.

Deng, C., & Rogers, L.J. (1998). Organisation of the tectorotundal and SP/IPS-rotundal projections in the chick. *The Journal of Comparative Neurology*, *394*(2), 171–185.

Eckhorn, R. (1994). Oscillatory and non-oscillatory synchronizations in the visual cortex and their possible roles in associations of visual features. *Progress in Brain Research*, *102*, 405–426.

Fricker, D., & Miles, R. (2000). EPSP amplification and the precision of spike timing in hippocampal neurons. *Neuron*, *28*(2), 559–569.

Friedrich, R., Habermann, C., Laurent, G. (2004). Multiplexing using synchrony in the zebrafish olfactory bulb. *Nature Neuroscience*, *7*, 862–871.

Gabernet, L., Jadhav, S., Feldman, D., Carandini, M., Scanzianiemail, M. (2005). Somatosensory integration controlled by dynamic thalamocortical feed-forward inhibition. *Neuron*, *48*(2), 315–327.

Gray, C. (1994). Synchronous oscillations in neuronal systems: mechanisms and functions. *Journal of Computational Neuroscience*, *1*, 11–38.

Guillery, R. (1967). Patterns of fiber degeneration in the dorsal lateral geniculate nucleus of the cat following lesions in the visual cortex. *Journal of Computational Neuroscience*, *130*(3), 197–221.

Jortner, R.A., Farivar, S.S., Laurent, G. (2007). A simple connectivity scheme for sparse coding in an olfactory system. *The Journal of Neuroscience*, *27*(7), 1659–1669.

Joshi, B., & Patel, M. (2013). Encoding with synchrony: Phase-delayed inhibition allows for reliable and specific stimulus detection. *Journal of Theoretical Biology*, *328*, 26–32.

Kyriazi, H., & Simons, D. (1993). Thalamocortical response transformations in simulated whisker barrels. *Journal of Neuroscience*, *13*(4), 1601–1615.

Laurent, G., & Davidowitz, H. (1994). Encoding of olfactory information with oscillating neural assemblies. *Science*, *265*, 1872–1875.

Leitch, B., Laurent, G., et al. (1996). GABAergic synapses in the antennal lobe and mushroom body of the locust olfactory system. *The Journal of Comparative Neurology*, *372*(4), 487–514.

Liu, X., Honda, C., Jones, E. (1995). Distribution of four types of synapse on physiologically identified relay neurons in the ventral posterior thalamic nucleus of the cat. *Journal of Computational Neuroscience*, *352*(1), 69–91.

Ly, C., Middleton, J., Doiron, B. (2012). Cellular and circuit mechanisms maintain low spike co-variability and enhance population coding in somatosensory cortex. *Frontiers in Computational Neuroscience*, *6*(7).

Marthy, V., & Fetz, E. (1992). Coherent 25- to 35-hz oscillations in the sensorimotor cortex of awake behaving monkeys. *Proceedings of the National Academy of Sciences of the United States of America*, *89*, 5670–5674.

Middleton, J., Omar, C., Doiron, B., Simons, D. (2012). Neural correlation is stimulus modulated by feedforward inhibitory circuitry. *The Journal of Neuroscience*, *32*(2), 506–518.

Mittmann, W., Koch, U., Häusser, M. (2005). Feed-forward inhibition shapes the spike output of cerebellar purkinje cells. *The Journal of Physiology*, *563*(2), 369–378.

Patel, M., & Joshi, B. (2013). Decoding synchronized oscillations within the brain: phase-delayed inhibition provides a robust mechanism for creating a sharp synchrony filter. *Journal of Theoretical Biology*, *334*, 13–25.

Patel, M., Rangan, A. V., Cai, D. (2009). A large-scale model of the locust antennal lobe. *Journal of Computational Neuroscience*, *27*(3), 553–567.

Patel, M., Rangan, A.V., Cai, D. (2013). Coding of odors by temporal binding within a model network of the locust antennal lobe. *Frontiers in Computational Neuroscience*, *7*(50), 1–18.

Patel, M., & Reed, M. (2013). Stimulus encoding within the barn owl optic tectum using gamma oscillations vs. spike rate: A modeling approach. *Network: Computation in Neural Systems*, *24*(2), 52–74.

Perez-Orive, J., Mazor, O., Turner, G.C., Cassenaer, S., Wilson, R.I., Laurent, G. (2002). Oscillations and sparsening of odor representations in the mushroom body. *Science*, *297*(5580), 359–365.

Pesavento, M., & Pinto, D. (2012). Network and neuronal membrane properties in hybrid networks reciprocally regulate selectivity to rapid thalamocortical inputs. *Journal of Neurophysiology*, *108*(9), 2452–2472.

Pesavento, M., Rittenhouse, C., Pinto, D. (2010). Response sensitivity of barrel neuron subpopulations to simulated thalamic input. *Journal of Neurophysiology*, *103*(6), 3001–3016.

Petersen, C. (2007). The functional organization of the barrel cortex. *Neuron*, *56*(2), 339–355.

Pinto, D., Brumberg, J., Simons, D. (2000). Circuit dynamics and coding strategies in rodent somatosensory cortex. *Journal of Neurophysiology*, *83*(3), 1158–1166.

Pinto, D., Brumberg, J., Simons, D., Ermentrout, G. (1996). A quantitative population model of whisker barrels: re-examining the wilson-cowan equations. *Journal of Computational Neuroscience*, *3*(3), 247–264.

Pinto, D., Hartings, J., Brumberg, J., Simons, D. (2003). Cortical damping: Analysis of thalamocortical response transformations in rodent barrel cortex. *Cerebral Cortex*, *13*(1), 33–44.

Pouille, F., & Scanziani, M. (2001). Enforcement of temporal fidelity in pyramidal cells by somatic feed-forward inhibition. *Science*, *293*(5532), 1159–1163.

Sridharan, D., Boahen, K., Knudsen, E.I. (2011). Space coding by gamma oscillations in the barn owl optic tectum. *Journal of Neurophysiology*, *105*(5), 2005–2017.

Sun, Q., Huguenard, J., Prince, D. (2006). Barrel cortex microcircuits: Thalamocortical feedforward inhibition in spiny stellate cells is mediated by a small number of fast-spiking interneurons. *Journal Neuroscience*, *26*(4), 1219–1230.

Tao, L., Shelley, M., McLaughlin, D., Shapley, R. (2004). An egalitarian network model for the emergence of simple and complex cells in visual cortex. *Proceedings of the National Academy of Sciences of the United States of America*, *101*(1), 366.

Temereanca, S., Brown, E., Simons, D. (2008). Rapid changes in thalamic firing synchrony during repetitive whisker stimulation. *The Journal of Neuroscience*, *28*(44), 11153–11164.

Temereanca, S., & Simons, D. (2004). Functional topography of corticothalamic feedback enhances thalamic spatial response tuning in the somatosensory whisker/barrel system. *Neuron*, *41*, 639–651.

Wang, Q., Webber, R., Stanley, G. (2010). Thalamic synchrony and the adaptive gating of information flow to cortex. *Nature Neuroscience*, *13*, 1534–1541.

Wehr, M., & Zador, A.M. (2003). Balanced inhibition underlies tuning and sharpens spike timing in auditory cortex. *Nature*, *426*(6965), 442–446.

Wilent, W., & Contreras, D. (2005). Dynamics of excitation and inhibition underlying stimulus selectivity in rat somatosensory cortex. *Nature Neuroscience*, *8*(10), 1364–1370.